

Prospects of detecting dark matter through cosmic-ray antihelium with the antiproton constraints

Nan Li^{*}, Chun-Cheng Wei[†], Yue-Liang Wu[‡] and Yu-Feng Zhou[§]

*CAS Key Laboratory of Theoretical Physics, Institute of Theoretical Physics,
Chinese Academy of Sciences, Beijing 100190, China.
University of Chinese Academy of Sciences, Beijing 100049, China.*

Abstract

Cosmic-ray (CR) antihelium can be an important observable for dark matter (DM) indirect searches due to extremely low secondary backgrounds towards low energies. In most DM models, the predicted CR antihelium flux is strongly correlated with that of CR antiprotons. Thus the upper limits on the DM annihilation cross sections from the current antiproton data can be used to place stringent limits on the maximal antihelium flux for the same model. Making use of the latest AMS-02 data on the antiproton to proton flux ratio and the coalescence model for the anti-nuclei formation, we obtain the maximal antihelium flux for typical DM annihilation final states such as $q\bar{q}$, $b\bar{b}$ and W^+W^- . The results are insensitive to the choices of DM density profiles and CR propagation models, but significantly dependent on the parameter of the coalescence momentum of the coalescence model. The prospects of detecting antihelium for the AMS-02 experiment is discussed. We show that with very optimistic assumptions on detection efficiency, acceptance and coalescence momentum, CR antihelium is within the reach of the AMS-02 experiment. The events which can be detected by AMS-02 are likely to have kinetic energy $T \gtrsim 30$ GeV and dominantly arise from secondary backgrounds rather than DM interactions.

^{*} linan2016@itp.ac.cn

[†] ccwei@itp.ac.cn

[‡] ylwu@itp.ac.cn

[§] yfzhou@itp.ac.cn

I. INTRODUCTION

Although the existence of dark matter (DM) as the dominant component of matter in the present-day Universe has been well established by observations, the particle nature of DM remains largely unknown. If DM particles in the Galactic halo can annihilate or decay into the standard model (SM) stable final states, they can make extra contributions to the fluxes of cosmic-ray (CR) particles, which can be probed by high precision DM indirect search experiments. Among many CR observables, CR antimatter, such as CR positrons, antiprotons and heavier anti-nuclei such as antideuteron and antihelium are considered to be relatively rare as they are dominated by CR secondaries produced by the collisions of primary CR particles onto the interstellar gas. Thus CR antiparticles are expected to be sensitive to extra contributions and can be important probes of DM.

In recent years, a number of experiments including AMS-02 have confirmed an unexpected rise in the CR positron flux above ~ 10 GeV [1–4]. DM annihilation or decay can be a possible explanation to this phenomena (see e.g. Refs. [5–8] for discussions related to the AMS-02 data) which is, however, subject to stringent constraints such as that from the observations of γ -rays from dwarf galaxies [9], the Galactic center [10], and the measurement of anisotropy in the cosmological microwave background (CMB) [11]. Another important observable is the CR antiproton which has been measured by a number of experiments such as PAMELA [12], BESS-polar II [13] and AMS-02 [14]. The high precision measurement of AMS-02 shows that in a large rigidity range from ~ 1 to 450 GV, the antiproton flux is in an overall agreement with the secondary origin of CR antiprotons, which can be used to place stringent constraints on the properties of DM particles (see e.g. Refs. [15–18]).

Despite the tiny production rates, heavier anti-nuclei such as antideuteron (\bar{D}) and antihelium-3 (${}^3\bar{\text{He}}$) can also be important probes of DM. With the increase of the atomic mass number A , the fluxes of anti-nuclei are expected to decrease rapidly due to smaller volume of phase space for the formation of anti-nuclei for both DM annihilation and secondary production. However, the secondary anti-nuclei are further suppressed by the high production threshold ($16m_p$ for \bar{D} and $30m_p$ for ${}^3\bar{\text{He}}$, where m_p is the proton mass) and the rapid falling of the primary CR proton flux at high energies (the proton flux scales with energy E as $E^{-2.75}$). The extremely low background makes it easier to single out the DM contributions in low energy region below ~ 10 GeV.

In a given DM model, the predicted fluxes of \bar{p} , \bar{D} and ${}^3\bar{\text{He}}$ are strongly correlated. The constraints on the DM properties from the antiproton data can be used to make predictions for the maximally possible fluxes of \bar{D} and ${}^3\bar{\text{He}}$ in the same DM model. Although the upper limits on the velocity-weighted DM annihilation cross section $\langle\sigma v\rangle$ obtained from the antiproton data strongly depend on the choice of DM density profiles and CR propagation models, the resulting predictions for the maximal fluxes of \bar{D} and ${}^3\bar{\text{He}}$ are highly insensitive to these choices. This is because the variation in the DM density profile and CR propagation model leads to a rescaling of the best-fit $\langle\sigma v\rangle$ in such a way that the same antiproton flux is reproduced.

The case of \bar{D} has been extensively discussed (for a recent review see e.g. [19]). In this work, we shall focus on the prospect of detecting ${}^3\bar{\text{He}}$ in the AMS-02 experiment,

motivated partly by the recent progresses made by AMS-02 in searching for heavier anti-nuclei [20]. We first update the upper limits on DM annihilation cross sections from the AMS-02 \bar{p}/p ratio, and then use the results to set maximal flux of ${}^3\bar{\text{He}}$ and number of events which could be observed by the AMS-02 detector in the whole lifetime of data taking. We use the Monte-Carlo (MC) event generator PYTHIA and the coalescence model to simulate the production of ${}^3\bar{\text{He}}$ from DM annihilation on an event-by-event basis, and then use the GALPROP code to full numerically calculate the propagation of ${}^3\bar{\text{He}}$ in the interstellar medium. The results show that with very optimistic estimates of detection efficiency and acceptance, and a relatively large coalescence momentum, CR antihelium is within the sensitivity of the AMS-02 experiment with a whole lifetime of data taking. We find that the events which can be detected by AMS-02 are likely to have kinetic energy $T \gtrsim 30$ GeV and dominantly arise from secondary backgrounds rather than DM annihilation.

This paper is organized as follows: In section II, we give a brief overview of the coalescence model. In section III, we use the Monte-Carlo event generator PYTHIA to simulate the production of ${}^3\bar{\text{He}}$ from the annihilation of DM particles. In section IV, we discuss the propagation of the anti-nuclei in the interstellar medium. In section V, we constrain the DM annihilation cross section using the AMS-02 \bar{p}/p ratio data. In section VI, we calculate the ${}^3\bar{\text{He}}$ flux at the top of atmosphere and discuss the detection prospect of the AMS-02 experiment. The conclusions are summarized in section VII.

II. THE COALESCENCE MODEL

We adopt the coalescence model to describe the formation of an anti-nucleus \bar{A} [21–23] from anti-nucleons. In this model a single parameter of coalescence momentum $p_0^{\bar{A}}$ is used to determine whether the anti-nucleons produced in a collision process can merge into an anti-nucleus. The basic idea is that the anti-nucleons are able to combine into an anti-nucleus only if a proper combination of the relative four-momenta of nucleons is less than $p_0^{\bar{A}}$. For example, in the case of antideuteron, the coalescence criterion is defined as

$$||k_{\bar{p}} - k_{\bar{n}}|| = \sqrt{(\Delta \vec{k})^2 - (\Delta E)^2} < p_0^{\bar{D}}, \quad (1)$$

where $k_{\bar{p}}$ and $k_{\bar{n}}$ are the four-momenta of \bar{p} and \bar{n} respectively, and $p_0^{\bar{D}}$ is the coalescence momentum of \bar{D} . In the case where the momentum distributions of \bar{p} and \bar{n} are isotropic and statistically independent, the energy spectrum of \bar{D} is related to that of \bar{p} and \bar{n} as

$$\gamma_{\bar{D}} \frac{d^3 N_{\bar{D}}}{d^3 \vec{k}_{\bar{D}}}(\vec{k}_{\bar{D}}) = \frac{1}{8} \cdot \frac{4}{3} \pi (p_0^{\bar{D}})^3 \cdot \gamma_{\bar{p}} \frac{d^3 N_{\bar{p}}}{d^3 \vec{k}_{\bar{p}}}(\vec{k}_{\bar{p}}) \gamma_{\bar{n}} \frac{d^3 N_{\bar{n}}}{d^3 \vec{k}_{\bar{n}}}(\vec{k}_{\bar{n}}), \quad (2)$$

where $\gamma_{\bar{D}, \bar{p}, \bar{n}}$ are the Lorentz factors, and $\vec{k}_{\bar{p}} \approx \vec{k}_{\bar{n}} \approx \vec{k}_{\bar{D}}/2$.

The coalescence criterion for the heavier anti-nuclei can be defined in a similar way as that of antideuteron [24]. For the case of ${}^3\bar{\text{He}}$, one can define the norms of the relative four-momenta between the three anti-nucleons as three lengths:

$$l_1 = ||k_1 - k_2||, \quad l_2 = ||k_2 - k_3||, \quad l_3 = ||k_1 - k_3||, \quad (3)$$

where k_1, k_2, k_3 are four-momenta of the three anti-nucleons respectively, and use these lengths to compose a triangle, and then make a circle with minimal diameter to envelope the triangle. The three anti-nucleons can successfully merge into an anti-nucleus only if the diameter of this circle is less than $p_0^{\overline{\text{He}}}$. If the three lengths form a right or obtuse triangle (i.e., $l_i^2 + l_j^2 \leq l_m^2$, for any $i, j, m \in \{1, 2, 3\}$), the minimal diameter equals to the longest side of the triangle, then the criterion can be simply written as $\max\{l_1, l_2, l_3\} < p_0^{\overline{\text{He}}}$. On the other hand, if the three lengths form an acute triangle ($l_i^2 + l_j^2 > l_m^2$, for all i, j, m), the minimal circle is just the circumcircle of this triangle, then the criterion can be expressed in terms of the diameter of the circumcircle:

$$d_{\text{circ}} = \frac{l_1 l_2 l_3}{\sqrt{(l_1 + l_2 + l_3)(-l_1 + l_2 + l_3)(l_1 - l_2 + l_3)(l_1 + l_2 - l_3)}} < p_0^{\overline{\text{He}}}. \quad (4)$$

An alternative way to define the coalescence criterion for ${}^3\overline{\text{He}}$ is requiring that the relative four-momentum of each pair of anti-nuclei is smaller than $p_0^{\overline{\text{He}}}$ [24, 25]:

$$||k_i - k_j|| < p_0^{\overline{\text{He}}} \quad (i, j = 1, 2, 3). \quad (5)$$

If the relative four-momenta form a right or obtuse triangle, This method is equivalent to the previous method, namely, $p_0^{\overline{\text{He}}}$ is determined by the longest side of the triangle. But for the case of acute triangles, this method predicts more anti-nuclei. The quantitative difference between these two methods will be discussed in the next section.

The spatially positions of particles also plays an important role in the formation of anti-nuclei, one should exclude the particle pairs which are not close enough to each other. As described in Ref. [24], this can be taken into account by setting all the particles with lifetime $\tau > 2$ fm to be stable, where 2 fm is approximately the scale of the wave function of ${}^3\overline{\text{He}}$.

III. THE INJECTION ENERGY SPECTRUM OF ${}^3\overline{\text{He}}$ FROM DM ANNIHILATION

The value of $p_0^{\overline{\text{A}}}$ should be determined by experimental data. In the case of antideuteron production, the value of $p_0^{\overline{\text{D}}}$ can be determined by reproducing the ALEPH results of the process $e^+e^- \rightarrow \overline{\text{D}} + X$ at the Z^0 resonance [26]. In this experiment, the production rate of antideuterons is $(5.9 \pm 1.8 \pm 0.5) \times 10^{-6}$ per hadronic Z^0 decay with $\overline{\text{D}}$ momenta ranging from 0.62 to 1.03 GeV and polar angle $\cos\theta < 0.95$. Through reproducing this result by using the event generator PYTHIA, it was found that $p_0^{\overline{\text{D}}} = 0.192 \pm 0.030$ GeV [27]. The value of $p_0^{\overline{\text{D}}}$ is known to be slightly dependent on the center-of-mass energy and the underlying process [19, 28]. As summarized in Ref. [19], other e^+e^- collider experiments at different center-of-mass energies lead to different values of p_0 . For instance, $\overline{\text{D}}$ productions at $\sqrt{s} = 9.46$ GeV through Υ resonances at CLEO gives $p_0^{\overline{\text{D}}} = 0.133$ GeV [29]; $\overline{\text{D}}$ productions at $\sqrt{s} = 10.58$ GeV through Υ resonances on $BABAR$ gives $p_0^{\overline{\text{D}}} = 0.135$ GeV [30]. In pp collisions, $\overline{\text{D}}$ productions at $\sqrt{s} = 53$ GeV on CERN ISR gives $p_0^{\overline{\text{D}}} = 0.152$ GeV [31, 32], while $\overline{\text{D}}$ productions at $\sqrt{s} = 7$ TeV at ALICE gives $p_0^{\overline{\text{D}}} = 0.230$ GeV [33]. In ep collisions, $\overline{\text{D}}$ productions at $\sqrt{s} = 318$ GeV at ZEUS [34] gives $p_0^{\overline{\text{D}}} = 0.236$ GeV. Considering the

resemblance to the dynamics of the annihilation of DM, we use value of $p_0^{\bar{D}}$ derived from the ALEPH data as a benchmark value.

For the case of antihelium production, it has been proposed to derive the value of $p_0^{\bar{\text{He}}}$ based on the relation between $p_0^{\bar{D}}$ and $p_0^{\bar{\text{He}}}$. There are two different approaches [24]:

(1) Determine p_0^{He} and p_0^D through fitting the inclusive spectra of deuterons, tritons and ^3He from the data on heavy-ion collisions at the Berkeley Bevalac collider [35], and then assume the relation $p_0^{\bar{\text{He}}}/p_0^{\bar{D}} = p_0^{\text{He}}/p_0^D$, which leads to [24]

$$p_{0A}^{\bar{\text{He}}} = \langle p_0^{\text{He}}/p_0^D \rangle p_0^{\bar{D}} = 1.28 p_0^{\bar{D}} = 0.246 \pm 0.038 \text{ GeV.} \quad (6)$$

(2) Use the theoretical relation $p_0 \sim \sqrt{E_b}$ [36], where E_b is the total nuclear binding energy, and obtain

$$p_{0B}^{\bar{\text{He}}} = \sqrt{E_b^{\bar{\text{He}}}/E_b^{\bar{D}}} p_0^{\bar{D}} = 0.357 \pm 0.059 \text{ GeV.} \quad (7)$$

In recent years, antihelium events have been observed in pp -collisions [28, 33, 37] and heavy-ion collisions at high energies [38, 39]. The ALICE experiment has reported antihelium-3 production rates at different regions of transverse momentum p_T in pp -collisions at $\sqrt{s} = 7 \text{ TeV}$, and obtained the corresponding values of the coalescence parameter B_3 [37]. In the isotropic limit, the value of B_3 can be straight forwardly translated into the value of $p_0^{\bar{\text{He}}}$. From the ALICE data, we find $p_0^{\bar{\text{He}}} \approx 0.228 - 0.378 \text{ GeV}$ for p_T/A in the range 0.4–2.0 GeV. These values are between that from the method (1) and (2). In this work, we shall use p_{0A} as a benchmark value to obtain the energy spectrum of $^3\bar{\text{He}}$. Note that, as expected from the coalescence model, the production rate of a nucleus with atomic mass number A should be proportional to $p_0^{3(A-1)}$ [21, 22], the variation of p_0 significantly changes the results of $^3\bar{\text{He}}$ production. We will give an estimation of the $^3\bar{\text{He}}$ flux for p_{0B} from the method (2) by rescaling the results from the method (1) in section VI.

There are two configurations of anti-nucleons which are possible to merge into an $^3\bar{\text{He}}$: direct formation of $\bar{p}\bar{n}$ or through the β -decay of antitriton \bar{T} ($\bar{p}\bar{n}\bar{n}$). However, as noted in Ref. [36], the direct formation channel is suppressed by Coulomb-repulsion between the two antiprotons, which is difficult to estimate quantitatively (see e.g. Ref. [40]). A simple approximation is to assume all the $^3\bar{\text{He}}$ are produced by the decay of antitriton. The energy loss from β -decay is negligible compares to the total energy of \bar{T} , so we assume that the energy spectrum of $^3\bar{\text{He}}$ is the same as \bar{T} formed in the coalescence model. The coalescence momentum of \bar{T} is also assumed to be the same as that of $^3\bar{\text{He}}$.

We use PYTHIA 8.223 [41, 42] to simulate the hadronization processes of DM annihilation, and adopt the coalescence model to describe the $^3\bar{\text{He}}$ formation on an event-by-event basis. We consider two Majorana DM particles annihilating into $q\bar{q}$ (q stands for u or d quark), $b\bar{b}$ and W^+W^- final states. Four possible values for the DM particle mass are considered: $m_\chi = 30, 100, 300$, and 1000 GeV . We generate $\mathcal{O}(10^{11})$ events for each case to produce enough $^3\bar{\text{He}}$ particles for calculating the injection energy spectrum. The final number of $^3\bar{\text{He}}$ particles produced is around $\mathcal{O}(10^4)$ for all the cases. In Fig. 1, we show the obtained energy spectra of $^3\bar{\text{He}}$ as a function of the scaled kinetic energy per nucleon $x = T/(nm_\chi)$, where n is the number of nucleons. Unlike $q\bar{q}$ or $b\bar{b}$ channels, in which a larger m_χ always leads to more $^3\bar{\text{He}}$ particles, in W^+W^- channel, the number of $^3\bar{\text{He}}$ decreases with the growing of DM

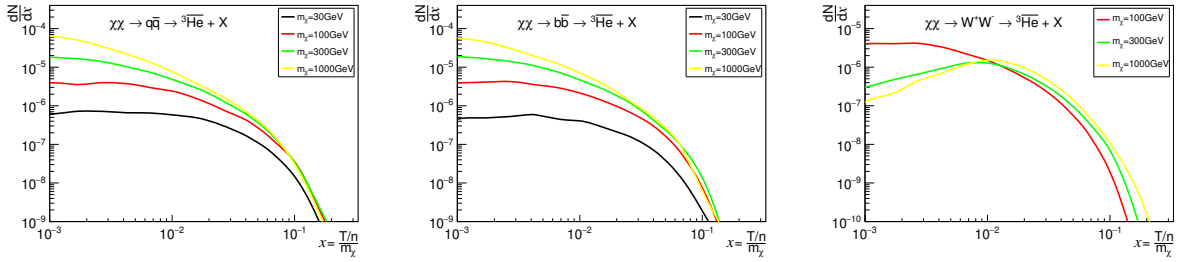


FIG. 1: Energy spectra of CR ${}^3\text{He}$ from DM annihilation as a function of scaled kinetic energy per nucleon $x = T/(nm_\chi)$ for different DM particle masses $m_\chi = 30 - 1000$ GeV. The left, middle and right panels correspond to DM particles annihilating into of $q\bar{q}$, $b\bar{b}$ and W^+W^- final states, respectively. The events are generated using PYTHIA [41, 42].

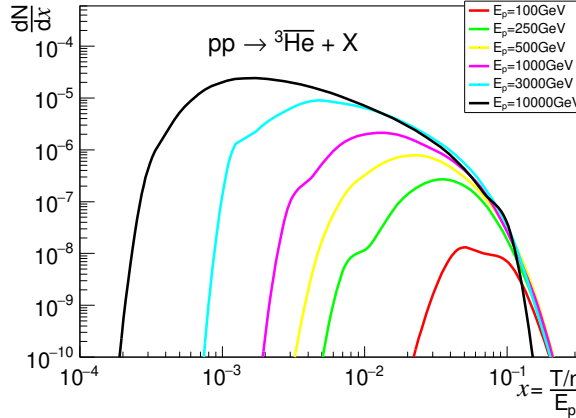


FIG. 2: Energy spectra of CR ${}^3\text{He}$ from pp -collisions for different total energies of incident protons $E_p = 100$ GeV–10 TeV. The target proton is at rest in the Galactic frame. The events are generated using PYTHIA [41, 42].

particles mass for $x \lesssim 10^{-2}$. The reason is that for the heavier DM particles, the produced W^+W^- particles are more energetic, and the decay products of W^+W^- are boosted to higher energies, which lead to the decrease of ${}^3\text{He}$ at lower energies.

The inelastic collisions between CR particles and the interstellar gas could also generate ${}^3\text{He}$, known as the secondaries. The main contribution of secondary ${}^3\text{He}$ is from the pp -collisions: $pp \rightarrow {}^3\text{He} + X$. We use PYTHIA 8.223 to simulate an energetic proton collides on a stationary proton with the incoming proton energy ranging from 100 GeV to 10 TeV, and then use the coalescence model to estimate the production of ${}^3\text{He}$. The energy spectra obtained for different energies of incident protons are shown in Fig. 2.

In order to quantitatively discuss the difference between the two coalescence criterions in Eqs. (4) and (5), we perform a Monte-Carlo test by using PYTHIA to simulate a pair of DM particles with $m_\chi = 1000$ GeV annihilating into $q\bar{q}$, and found that the method of Eq. (4) we used produces about 13% fewer ${}^3\text{He}$ particles compares to the method of Eq. (5). The

difference found in our calculation is larger than the previous estimation of $\sim 6\%$ in Ref. [24] which assumed an isotropic momenta distribution. Nevertheless, the difference between the two methods would not affect the conclusion significantly.

It is worth noting that, as discussed in Ref. [19], the choice of the MC event generator can also affect the results. Besides PYTHIA, other MC event generators, such as **Herwig** [43], **DPMJET** [44], **QGSJET** [45, 46], **EPOS** [47] and **EPOS-LHC** [48] are also widely used. The MC event generator PYTHIA is tuned for simulating the collision at high energies, and they may not well reproduce the results of pp collisions at lower center-of-mass energies $\sqrt{s} \sim 10$ GeV, which is the typical scale of the production of secondary ${}^3\overline{\text{He}}$. It was suggested in Ref. [19] and [49] that the DPMJET, the QGSJET and the EPOS MC generators which are tuned for fitting the collider data at low energies, may be more suitable for calculating the secondary contributions.

IV. THE PROPAGATION OF ${}^3\overline{\text{He}}$

The propagation of CR anti-nuclei can be described by the diffusion model in which the diffusion halo is assumed to be a cylinder with radius $r_h \approx 20$ kpc and half-height $z_h = 1 \sim 10$ kpc. The diffusion equation of CR charged particles can be written as [50, 51]:

$$\frac{\partial f}{\partial t} = q(\vec{r}, p) + \vec{\nabla} \cdot (D_{xx} \vec{\nabla} f - \vec{V}_c f) + \frac{\partial}{\partial p} p^2 D_{pp} \frac{\partial}{\partial p} \frac{1}{p^2} f - \frac{\partial}{\partial p} \left[\dot{p} f - \frac{p}{3} (\vec{\nabla} \cdot \vec{V}_c) f \right] - \frac{1}{\tau_f} f - \frac{1}{\tau_r} f, \quad (8)$$

where $f(\vec{r}, p, t)$ is the number density per unit of particle momentum p at the position \vec{r} , and $q(\vec{r}, p)$ is the source term. D_{xx} is the energy dependent spatial diffusion coefficient which is parameterized as $D_{xx} = \beta D_0 (R/R_0)^\delta$, where $R = p/(Ze)$ is the rigidity of the cosmic-ray particle with electric charge Ze , δ is the spectral power index which can take two different values $\delta = \delta_{1(2)}$ when R is below (above) a reference rigidity R_0 , D_0 is a constant normalization coefficient, and $\beta = v/c$ is the velocity of CR particles. \vec{V}_c is the convection velocity, which is related to the galactic wind. Diffusive re-acceleration is described as diffusion in momentum space, and is described by the parameter D_{pp} which can be parameterized as $D_{pp} = p^2 V_a^2 / (9D_{xx})$, where V_a is the Alfvèn velocity which characterises the propagation of weak disturbances in a magnetic field. $\dot{p} \equiv dp/dt$ is the momentum loss rate, τ_f and τ_r are the time scales of particle fragmentation and radioactive decay respectively. The steady-state diffusion condition is achieved by setting $\partial f / \partial t = 0$. For boundary conditions, it is assumed that the number densities of CR particles are vanishing at the boundary of the halo: $f(r_h, z, p) = f(r, \pm z_h, p) = 0$. We use the code **GALPROP v54** [52–56] to numerically solve the diffusion equation of Eq. (8).

For primary ${}^3\overline{\text{He}}$ produced by the annihilation of Majorana DM particles, the source term can be written as follows:

$$q_{\overline{\text{He}}}(\vec{r}, p) = \frac{\rho_{\text{DM}}^2(\vec{r})}{2m_\chi^2} \langle \sigma v \rangle \frac{dN_{\overline{\text{He}}}}{dp}, \quad (9)$$

where $\rho_{\text{DM}}(\vec{r})$ is the DM energy density, $\langle \sigma v \rangle$ is the thermally averaged annihilation cross section of DM and $dN_{\overline{\text{He}}}/dp$ is the injection spectrum of $\overline{\text{He}}$ discussed in the previous section.

The source term for the secondary ${}^3\overline{\text{He}}$ is given by:

$$q(\vec{r}, p) = \beta c n_{\text{H}}(\vec{r}) \int \sigma_{pp}^{\text{inel}}(p') \frac{dN_{\overline{\text{He}}}(p, p')}{dp} n_p(\vec{r}, p') dp' , \quad (10)$$

where n_{H} is the number density of the interstellar hydrogen, n_p is the number density of CR proton per unit momentum, $\sigma_{pp}^{\text{inel}}(p')$ is the inelastic cross section of pp -collision, and $dN_{\overline{\text{He}}}(p, p')/dp$ is the energy spectrum of ${}^3\overline{\text{He}}$ in the pp -collision with the momentum of the incoming proton is p' . It is assumed that the primary CR nucleus injection spectra have a broken power law, with the injection index $\gamma_p = \gamma_{p1}(\gamma_{p2})$ for the nucleus rigidity R_p below (above) a reference value R_{ps} . The spatial distribution of the interstellar gas and the primary sources of CR nuclei are taken from Ref. [52]. In the calculation of the ${}^3\overline{\text{He}}$ flux, we neglect the subdominant tertiary contributions, as they are only compatible with the background towards kinetic energies below $0.4 - 0.6$ GeV/n [57].

The inelastic interaction rate of the scattering between ${}^3\overline{\text{He}}$ and the interstellar gases is related to the τ_f in Eq. (8) by $\Gamma_{\text{int}} = 1/\tau_f$, and is written as [24, 25]

$$\Gamma_{\text{int}} = (n_{\text{H}} + 4^{2/3} n_{\text{He}}) v \sigma_{\overline{\text{He}}, p} , \quad (11)$$

where n_{H} and n_{He} are the number densities of interstellar hydrogen and helium respectively, $4^{2/3}$ is the geometrical factor, v is the velocity of ${}^3\overline{\text{He}}$ relative to interstellar gases, and $\sigma_{\overline{\text{He}}, p}$ is the total inelastic cross section between ${}^3\overline{\text{He}}$ and protons. The He/H number density ratio of the interstellar gas is taken to be 0.11 from Ref. [52].

Since the experimental data of the cross section $\sigma_{\overline{\text{He}}, p}$ is currently not available, we assume the relation $\sigma_{\overline{\text{He}}, p} = \sigma_{\text{He}, \bar{p}}$ by CP-invariance. For an incoming nucleus with atomic number A , charge number Z and kinetic energy T which collides on a stationary antiproton, the total inelastic cross sections are parameterized by the following formula [53]:

$$\sigma_{A\bar{p}}^{\text{tot}} = A^{2/3} [48.2 + 19 x^{-0.55} + (0.1 - 0.18 x^{-1.2})Z + 0.0012 x^{-1.5} Z^2] \text{ mb}, \quad (12)$$

where $x = T/(A \cdot \text{GeV})$. By substituting $A = 3$ and $Z = 2$, we obtain the cross section $\sigma_{\overline{\text{He}}, p}$.

The inelastic cross section for pp -collisions, which is required in Eq. (10) is taken from Ref. [58] (referred to as Tan & Ng) as the default settings in the GALPROP code, which is given by:

$$\sigma_{pp}^{\text{inel}} = 32.2 [1 + 0.0273 U + 0.01 U^2 \theta(U)] \text{ mb} \times \begin{cases} (1 + 2.62 \times 10^{-3} x^{-C})^{-1}, & 0.3 \leq x < 3; \\ 1, & x \geq 3; \end{cases} \quad (13)$$

where $x = T/\text{GeV}$, $U = \ln((x + m_p)/200)$, m_p is the mass of proton, $C = 17.9 + 13.8 \ln x + 4.41 \ln^2 x$ and $\theta(U)$ is the Heaviside step function. For $x < 0.3$, the inelastic cross section is vanishing $\sigma_{pp}^{\text{inel}} = 0$. This formula is different from that used in PYTHIA, but the numerical difference between the two is negligible, which is illustrated in Fig. 3.

When anti-nuclei propagate in the heliosphere, the magnetic field of solar system and the solar wind modulate the spectrum of the particles. We use the force-field approximation to quantify the effects of solar modulation [59]:

$$\Phi_{A,Z}^{\text{TOA}}(T_{\text{TOA}}) = \left(\frac{2m_A T_{\text{TOA}} + T_{\text{TOA}}^2}{2m_A T_{\text{IS}} + T_{\text{IS}}^2} \right) \Phi_{A,Z}^{\text{IS}}(T_{\text{IS}}), \quad (14)$$

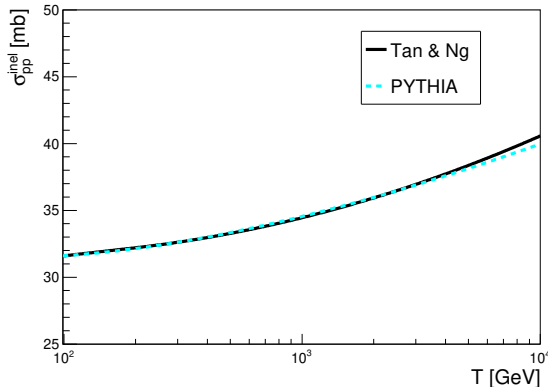


FIG. 3: Differential inelastic cross sections of pp -collisions as a function of the kinetic energy of the incident proton. The solid (dashed) curve is calculated using the formula of Eq. (13) (PYTHIA 8.223).

where Φ stands for the flux of the CR particles, which is related to the density function f by $\Phi = vf/(4\pi)$, “TOA” stands for the value at the top of the atmosphere of the earth, “IS” stands for the value at the boundary between the interstellar and the heliosphere and m is the mass of the nucleus. T_{IS} is related to T_{TOA} as $T_{\text{IS}} = T_{\text{TOA}} + e\phi_F|Z|$. In this work, the value of the Fisk potential is fixed at $\phi_F = 550$ MV.

V. THE UPPER LIMIT OF DM ANNIHILATION CROSS SECTION

The DM annihilation cross sections for annihilation channels such as $q\bar{q}$, $b\bar{b}$ and W^+W^- are constrained by the antiproton data, and the constraints can strongly affect the predictions for the ${}^3\text{He}$ flux. In Ref. [16], the 95% CL upper limit of DM annihilation cross section was obtained based on the preliminary AMS-02 \bar{p}/p data released in 2015 [60]. In this work, we update the constraints in Ref. [16] with the updated AMS-02 \bar{p}/p data published in 2016 [14] for four diffusive re-acceleration (DR) propagation models: the “conventional” model [54, 56], the “MIN”, “MED” and “MAX” models [61]. The “Conventional” model is commonly adopted as a benchmark model by many experimental collaborations. The “MIN”, “MED” and “MAX” models are obtained from a global fit to the proton and B/C data of AMS-02 using the **GALPROP** code. These models represent the typically minimal, median and maximal antiproton fluxes after considering the uncertainties in the propagation models. Note that these models are not the ones proposed in Ref. [62] which are based on semi-analytical approaches. The value of parameters of the four models are listed in Tab. I. For each propagation model, four commonly used DM profiles are considered: the Navarro-Frenk-White (NFW) profile [63], the Isothermal profile [64], the Moore profile [65, 66], and the Einasto profile [67]. The details of deriving the upper limits can be found in Ref. [16]. In this updated analysis, the primary nuclei source term is normalized to reproduce the AMS-02 proton flux at a reference kinetic energy $T = 100$ GeV. The updated results for $q\bar{q}$, $b\bar{b}$ and W^+W^- are presented in Fig. 4, Fig. 5 and Fig. 6 respectively. We find that the

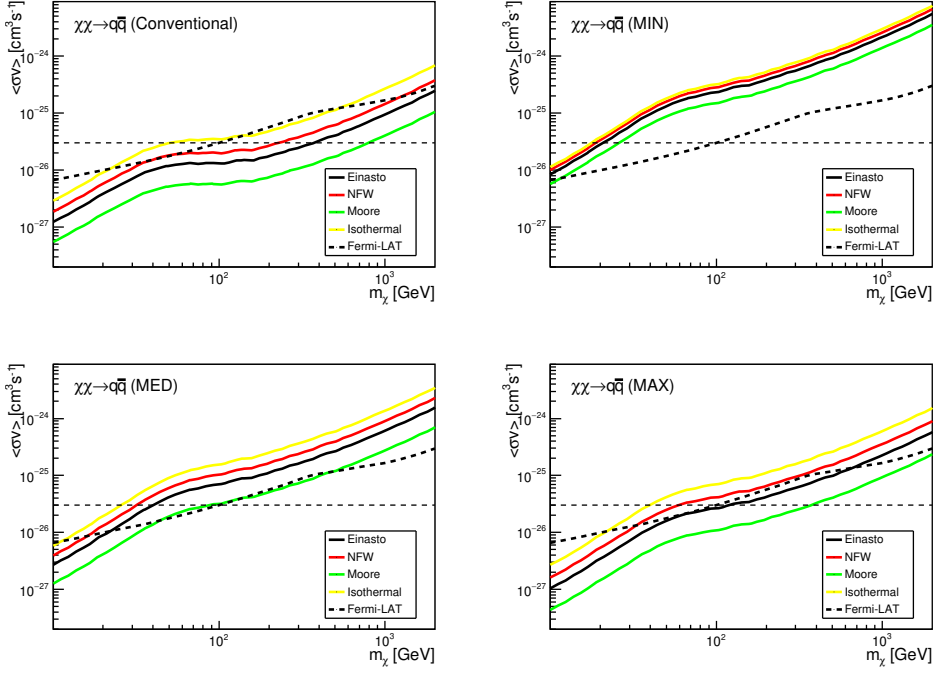


FIG. 4: Upper limits on the cross sections for DM particle annihilation into $q\bar{q}$ final states at 95% C.L. from the AMS-02 \bar{p}/p data in the “Conventional” (upper left), “MIN” (upper right), “MED” (lower left) and “MAX” (lower right) propagation models. Four DM profiles NFW [63], Isothermal [64], Einasto [67] and Moore [65, 66] are considered. The upper limits from the Fermi-LAT 6-year gamma-ray data of the dwarf spheroidal satellite galaxies of the Milky Way [9] are also shown. The horizontal line indicates the typical thermal annihilation cross section $\langle\sigma v\rangle = 3 \times 10^{-26} \text{ cm}^3 \cdot \text{s}^{-1}$.

new upper limits are comparable with previous ones, but the constraints for the DM with $m_\chi \lesssim 100 \text{ GeV}$ are more stringent. In Fig. 4-6, the upper limits from the Fermi-LAT 6-years gamma-ray data of the dwarf spheroidal galaxies [9] are also shown for a comparison.

Model	$r_h(\text{kpc})$	$z_h(\text{kpc})$	D_0	$R_0(\text{GV})$	δ_1/δ_2	$V_a(\text{km/s})$	$R_{ps}(\text{GV})$	γ_{p1}/γ_{p2}
Conventional	20	4.0	5.75	4.0	0.34/0.34	36.0	9.0	1.82/2.36
MIN	20	1.8	3.53	4.0	0.3/0.3	42.7	10.0	1.75/2.44
MED	20	3.2	6.50	4.0	0.29/0.29	44.8	10.0	1.79/2.45
MAX	20	6.0	10.6	4.0	0.29/0.29	43.4	10.0	1.81/2.46

TABLE I: Values of the main parameters in the “Conventional” propagation model [54, 56], and that in the “MIN”, “MED” and “MAX” models [61]. The parameter D_0 is in units of $10^{28} \text{ cm}^2 \cdot \text{s}^{-1}$.

It can be seen that with the growth of the DM mass, the upper limits become weaker, and can be larger than the typical thermal relic cross section $\langle\sigma v\rangle = 3 \times 10^{-26} \text{ cm}^3 \cdot \text{s}^{-1}$ by several orders of magnitude. The upper limits for $\chi\chi \rightarrow q\bar{q}$ channel are the most stringent

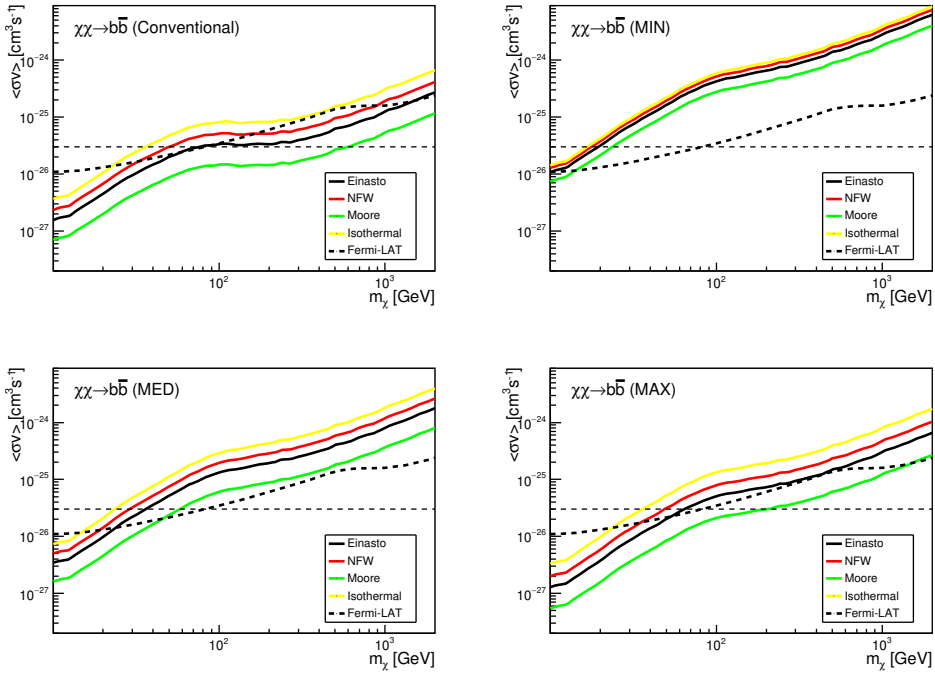


FIG. 5: The same as Fig. 4, but for $b\bar{b}$ annihilation final states.

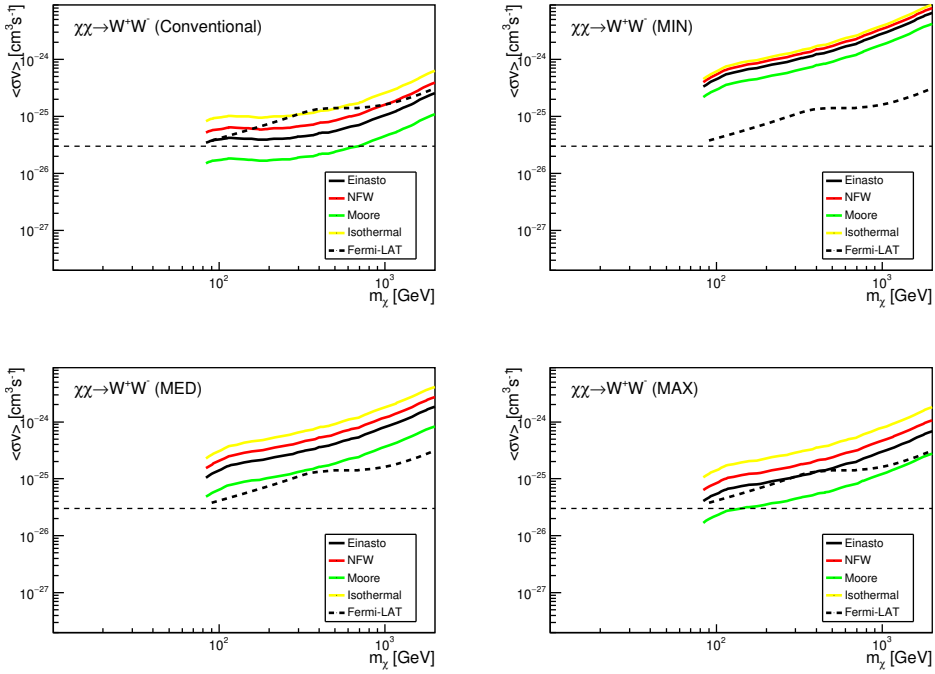


FIG. 6: The same as Fig. 4, but for W^+W^- annihilation final states.

among the three types of final states. For the “Conventional” (“MIN”) propagation model, we get more (less) stringent constraints than that obtained from the Fermi-LAT gamma-ray data for all the DM masses. For the “MED” and the “MAX” model, our upper limits are comparable with that from the Fermi-LAT, but more stringent limits are obtained for smaller DM mass.

VI. PROSPECTS OF DETECTING ${}^3\overline{\text{He}}$ EVENTS AT AMS-02

From the coalescence model, it is expected that the production of ${}^3\overline{\text{He}}$ is strongly correlated with that of antiproton. Thus the upper limits on the DM annihilation cross section obtained from the antiproton data can be used to set upper bounds on the flux of ${}^3\overline{\text{He}}$. The major uncertainties in the predicted ${}^3\overline{\text{He}}$ fluxes arise from the following sources:

- The uncertainty in the choice of DM density profiles. For a fixed DM annihilation cross section, the choice of DM profiles can change the final flux up to about an order of magnitude.
- The uncertainty in the choice of different propagation models. As shown in previous works [24, 25], this can change the flux of ${}^3\overline{\text{He}}$ up to two orders of magnitude for a fixed DM annihilation cross section.
- The uncertainty in the coalescence momentum $p_0^{\overline{\text{He}}}$. As discussed in Sec. III, the production rate of ${}^3\overline{\text{He}}$ is approximately proportional to $(p_0^{\overline{\text{He}}})^6$. Thus the difference between $p_{0A}^{\overline{\text{He}}}$ and $p_{0B}^{\overline{\text{He}}}$ can affect the results roughly by an order of magnitude.

An advantage of using the antiproton data to constrain the ${}^3\overline{\text{He}}$ flux is that the obtained limits are insensitive to the DM density profile, as the variation in the DM profile mainly results in a rescaling of the best-fit $\langle\sigma v\rangle$ in such a way that the same antiproton flux is reproduced. In the left panel of Fig. 7, we show the upper limits on the ${}^3\overline{\text{He}}$ flux for the four different DM profiles in the same propagation model with $q\bar{q}$ final states and the DM mass fixed at 300 GeV. It can be clearly seen that the dependence on the DM profile is very small. The constraints are also insensitive to the choice of propagation models, provided that they give the same secondary antiproton background. In the right panel of Fig. 7, we show the upper limits on ${}^3\overline{\text{He}}$ flux for the four different propagation models with the same DM profile. For the models give nearly the same secondary background such as the “MIN”, “MED” and “MAX” models, the obtained limits are nearly the same. In the “conventional” model, the predicted secondaries are slightly higher than that in the “MIN”, “MED” and “MAX” models, which results in a decrease of $\sim 30\%$ in the predicted ${}^3\overline{\text{He}}$ flux. Note, however, that compared with the “MIN”, “MED” and “MAX” models, the “conventional” model does not fit the AMS-02 proton data very well [16].

In this approach, the uncertainty in $p_0^{\overline{\text{He}}}$ becomes the dominant source of the uncertainty in the theoretical predictions. In Fig. 8 we show the predicted upper limits on the ${}^3\overline{\text{He}}$ flux for more DM annihilation final states including W^+W^- and $b\bar{b}$ and typical DM masses in the range 30 GeV–1 TeV with the uncertainties in $p_0^{\overline{\text{He}}}$ taken into account. Despite the significant

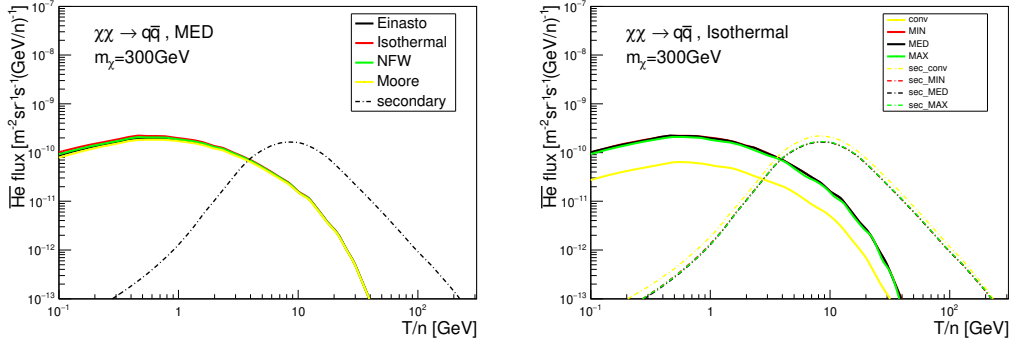


FIG. 7: Left) Predicted maximal ${}^3\overline{\text{He}}$ fluxes (solid curves) as a function of kinetic energy per nucleon from DM annihilation into $q\bar{q}$ final states in the MED propagation model with four different DM profiles NFW [63], Isothermal [64], Einasto [67] and Moore [65, 66]. The DM particle mass is fixed at $m_\chi = 300$ GeV. The secondary ${}^3\overline{\text{He}}$ flux is also shown for a comparison. The value of coalescence momentum is set to be $p_{0A}^{\overline{\text{He}}} = 0.246 \pm 0.038$ GeV. Right) The same as left, but for four different propagation models “Conventional” [54, 56], MIN, MED and MAX [61] with “Isothermal” DM profile.

uncertainties, one can still see that the secondary background is negligibly small for kinetic energy T below ~ 1 GeV, which suggests that any detected ${}^3\overline{\text{He}}$ with kinetic energy lower than ~ 1 GeV would be a strong hint for exotic contributions such as that from DM.

Detecting $\overline{\text{He}}$ is one of the major scientific objectives of the AMS-02 experiment. In this work we give an estimation of the number of ${}^3\overline{\text{He}}$ events that can be observed by AMS-02 after the whole lifetime of the experiment (assumed to be 18 years) under the most optimistic assumptions. The number of ${}^3\overline{\text{He}}$ events observed by a detector can be written as

$$N = \int_{T_{\min}}^{T_{\max}} \eta \Phi_{\overline{\text{He}}} \mathcal{A} t dT, \quad (15)$$

where $\Phi_{\overline{\text{He}}}$ is the flux of ${}^3\overline{\text{He}}$, \mathcal{A} is the acceptance of ${}^3\overline{\text{He}}$ which is assumed to be same as the geometric acceptance of the AMS-02 detector $\mathcal{A} \approx 0.5 \text{ m}^2 \cdot \text{sr}$, η is the detecting efficiency which is assumed to be unity, and $t \approx 18$ years is the total time of exposure AMS-02. The integration lower and upper limits are set to be $T_{\min}/n = 0.1$ GeV and $T_{\max}/n = 1$ TeV, respectively.

In Tab. II, we show the predicted maximal total number of antihelium events for four different annihilation channels, DM particle masses and the two values of coalescence momentum $p_{0A}^{\overline{\text{He}}}$ and $p_{0B}^{\overline{\text{He}}}$. The flux for the case of $p_{0B}^{\overline{\text{He}}}$ is obtained by rescaling that of the case of $p_{0A}^{\overline{\text{He}}}$ by the relation $\Phi_{\overline{\text{He}}} \sim (p_0^{\overline{\text{He}}})^6$. The expected secondary backgrounds are also shown. As shown in the table, if the coalescence momentum is set to $p_{0A}^{\overline{\text{He}}}$, in the most optimistic case the expected total number of events is around $1 \sim 2$. However, if it is set to $p_{0B}^{\overline{\text{He}}}$, the expected total number of events can reach $\mathcal{O}(10)$. In both cases, the total number of events are dominated by the secondaries.

A more realistic estimation of the prospective 18-year ${}^3\overline{\text{He}}$ detecting sensitivity of AMS-02 was given in terms of $\overline{\text{He}}/\text{He}$ flux ratio in Ref. [68], where He stands for the sum of ${}^3\text{He}$ and

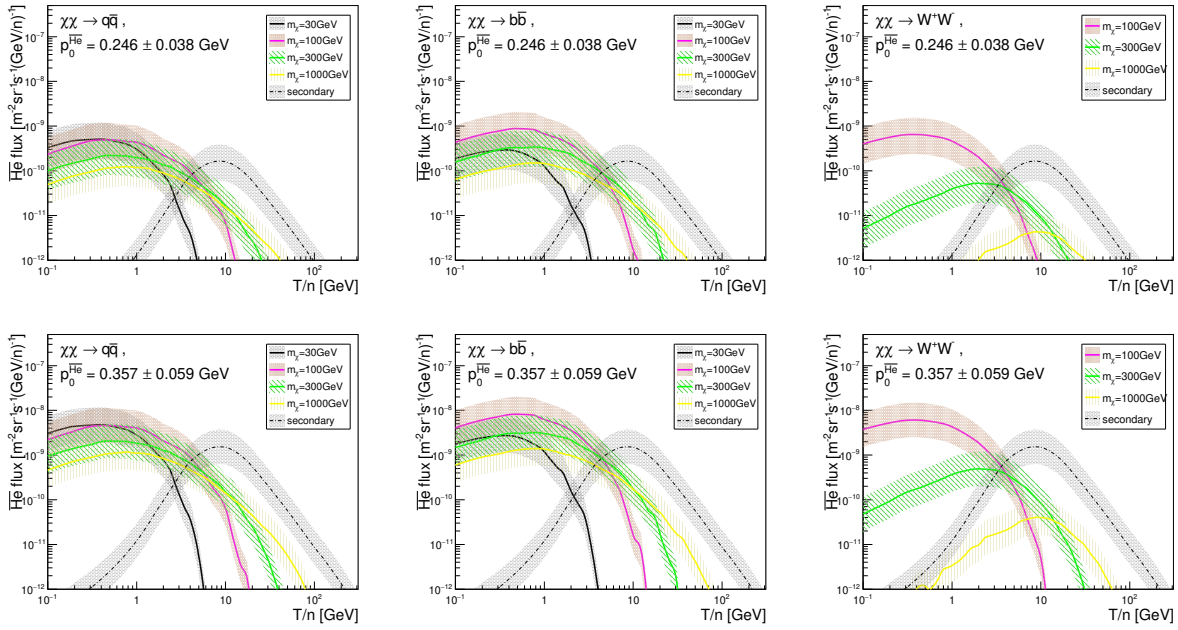


FIG. 8: Upper panels) Predicted maximal CR ${}^3\text{He}$ fluxes (solid curves) as a function of kinetic energy per nucleon from DM annihilation into $q\bar{q}$ (left panel), $b\bar{b}$ (middle panel) and W^+W^- (right panel) final states with different DM particle masses. The coalescence momentum is set to be $p_{0A}^{\text{He}} = 0.246 \pm 0.038$ GeV. The shaded bands represent the uncertainties in the coalescence momentum. The MED propagation model and the “Isothermal” DM profile are adopted in the calculation. The secondary ${}^3\text{He}$ flux (dashed curve) is also shown for a comparison. Lower panels) The same as the upper panels, but with a different value of the coalescence momentum $p_{0B}^{\text{He}} = 0.357 \pm 0.059$ GeV.

${}^4\text{He}$. For a comparison, we also show the predicted $\overline{\text{He}}/\text{He}$ in the “MED” propagation model with the “Isothermal” DM profile for different annihilation channels, DM particle masses, and coalescence momenta in Fig. 9. As can be seen from the figure, for the case with relatively small coalescence momentum of p_{0A}^{He} , the possibility of detecting $\overline{\text{He}}$ is marginal, while for relatively large coalescence momentum of p_{0B}^{He} , it is quite possible that some events can be observed. The events which can be observed are likely to have kinetic energy $T/n \gtrsim 10$ GeV or $T \gtrsim 30$ GeV, and are dominantly arising from the secondary backgrounds. Recently, the AMS-02 collaboration has reported preliminary hints of antihelium events [69]. For instance, a candidate event of ${}^3\text{He}$ with momentum 40.3 ± 2.9 GeV is shown. Such an event corresponds to a kinetic energy per nucleon $T/n \approx 12.5$ GeV, which is close to the peak of the energy spectrum of the secondary ${}^3\text{He}$. Thus it would be more like a hint of secondary backgrounds. In a recent analysis, it was claimed that such candidate events can be attributed to the annihilation or decay of Galactic DM [70], which however, did not take the secondary backgrounds into account.

	m_χ	$\chi\chi \rightarrow q\bar{q}$	$\chi\chi \rightarrow b\bar{b}$	$\chi\chi \rightarrow W^+W^-$
DM	30 GeV	0.217 (2.027)	0.098 (0.915)	—
	100 GeV	0.426 (3.979)	0.643 (6.006)	0.381 (3.559)
	300 GeV	0.292 (2.728)	0.428 (3.998)	0.113 (1.056)
	1000 GeV	0.225 (2.102)	0.266 (2.485)	0.031 (0.292)
Secondary		0.947 (8.846)		

TABLE II: The prospective maximal number of ${}^3\overline{\text{He}}$ particles can be detected by AMS-02 after 18 years of data taking under the most optimistic assumptions (see text for details). The DM contributions with the constraints from the AMS-02 antiproton data for four different DM masses $m_\chi = 30 - 1000$ GeV and three annihilation final states $q\bar{q}$, $b\bar{b}$ and W^+W^- are shown. The coalescence momentum is set to $p_{0A}^{\overline{\text{He}}}$. The MED propagation model and the “Isothermal” DM profile are adopted in the calculation. The secondary ${}^3\overline{\text{He}}$ are also shown for a comparison. The numbers in the brackets correspond to a larger coalescence momentum of $p_{0B}^{\overline{\text{He}}}$.

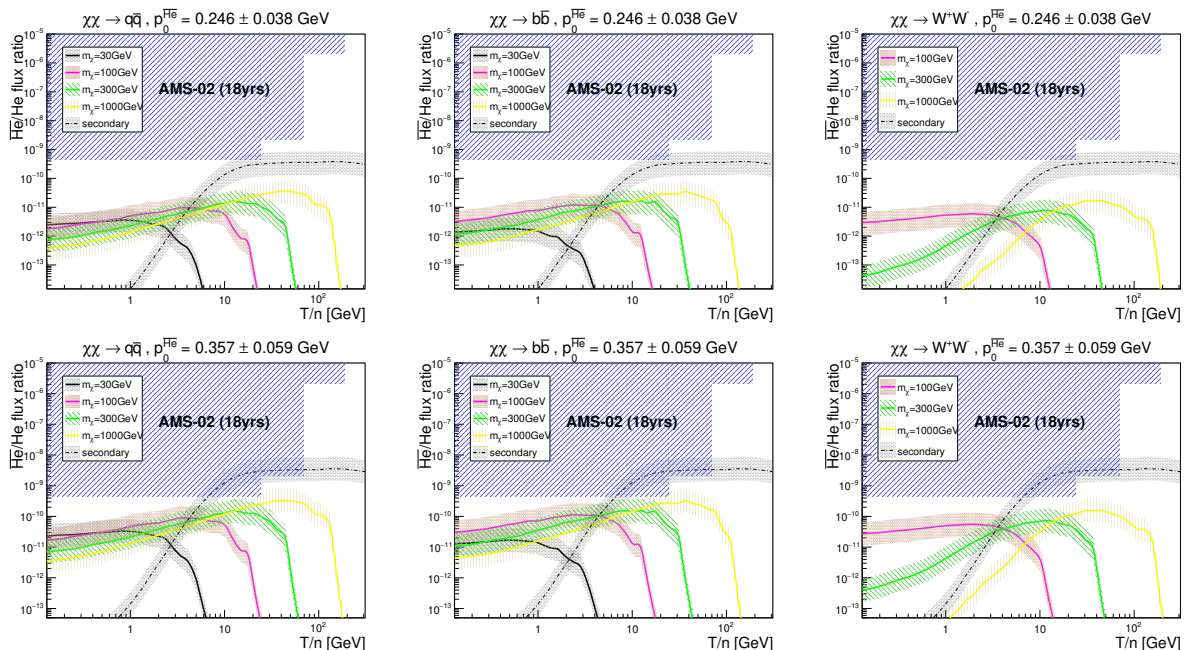


FIG. 9: Upper panels) Predicted maximal $\overline{\text{He}}/\text{He}$ flux ratio (solid curves) as a function of kinetic energy per nucleon from DM annihilation into $q\bar{q}$ (left panel), $b\bar{b}$ (middle panel) and W^+W^- (right panel) final states with different DM particle masses. The coalescence momentum is set to be $p_{0A}^{\overline{\text{He}}} = 0.246 \pm 0.038$ GeV. The shaded bands represent the uncertainties in the coalescence momentum. The MED propagation model and the “Isothermal” DM profile are adopted in the calculation. The secondary contributions (dashed curve) are also shown for a comparison. The blue shaded regions represent the detection sensitivity of AMS-02 at 95% C.L., after 18 years of data taking [68]. Lower panels) The same as the upper panels, but with a different value of the coalescence momentum $p_{0B}^{\overline{\text{He}}} = 0.357 \pm 0.059$ GeV.

VII. CONCLUSION AND DISCUSSIONS

In summary, motivated partly by the recent progresses made by AMS-02 in searching for heavier anti-nuclei, we have discussed the prospect of detecting ${}^3\overline{\text{He}}$ in the AMS-02 experiment under the constraints from the AMS-02 antiproton data. We have updated the upper limits on DM annihilation cross sections from the AMS-02 \bar{p}/p ratio, and then used the results to set limits on the ${}^3\overline{\text{He}}$ flux and number of events which could be observed by AMS-02 in the whole lifetime of data taking. We have used the coalescence model to simulate the production of ${}^3\overline{\text{He}}$ from DM annihilation on an event-by-event basis, and used the **GALPROP** code to calculate the propagation of ${}^3\overline{\text{He}}$ in the interstellar medium. The results show that with very optimistic estimates of detection efficiency and acceptance, and a relatively large coalescence momentum, CR antihelium is within the sensitivity of the AMS-02 experiment with a whole lifetime of data taking. The number of events can reach $\mathcal{O}(10)$, depending on the value of the coalescence momentum. We have also shown that the events which can be detected by AMS-02 are likely to have kinetic energy $T \gtrsim 30$ GeV and dominantly arise from secondary backgrounds rather than DM annihilation.

Acknowledgments

This work is supported in part by the NSFC under Grants No. 11690022, No. 11475237, No. 11335012, No. U1738209 and No. 11851303, the National Key R&D Program of China No. 2017YFA0402204, and the CAS key research program No. XDB23030100, No. QYZDY-SSW-SYS007.

- [1] J. J. Beatty *et al.*, “New measurement of the cosmic-ray positron fraction from 5 to 15-GeV,” *Phys. Rev. Lett.* **93** (2004) 241102, [arXiv:astro-ph/0412230](https://arxiv.org/abs/astro-ph/0412230) [astro-ph].
- [2] **PAMELA** Collaboration, O. Adriani *et al.*, “An anomalous positron abundance in cosmic rays with energies 1.5-100 GeV,” *Nature* **458** (2009) 607–609, [arXiv:0810.4995](https://arxiv.org/abs/0810.4995) [astro-ph].
- [3] **Fermi-LAT** Collaboration, M. Ackermann *et al.*, “Measurement of separate cosmic-ray electron and positron spectra with the Fermi Large Area Telescope,” *Phys. Rev. Lett.* **108** (2012) 011103, [arXiv:1109.0521](https://arxiv.org/abs/1109.0521) [astro-ph.HE].
- [4] **AMS** Collaboration, L. Accardo *et al.*, “High Statistics Measurement of the Positron Fraction in Primary Cosmic Rays of 0.5–500 GeV with the Alpha Magnetic Spectrometer on the International Space Station,” *Phys. Rev. Lett.* **113** (2014) 121101.
- [5] J. Kopp, “Constraints on dark matter annihilation from AMS-02 results,” *Phys. Rev.* **D88** (2013) 076013, [arXiv:1304.1184](https://arxiv.org/abs/1304.1184) [hep-ph].
- [6] L. Bergstrom, T. Bringmann, I. Cholis, D. Hooper, and C. Weniger, “New limits on dark matter annihilation from AMS cosmic ray positron data,” *Phys. Rev. Lett.* **111** (2013) 171101, [arXiv:1306.3983](https://arxiv.org/abs/1306.3983) [astro-ph.HE].

[7] A. Ibarra, A. S. Lamperstorfer, and J. Silk, “Dark matter annihilations and decays after the AMS-02 positron measurements,” *Phys. Rev.* **D89** no. 6, (2014) 063539, [arXiv:1309.2570 \[hep-ph\]](https://arxiv.org/abs/1309.2570).

[8] H.-B. Jin, Y.-L. Wu, and Y.-F. Zhou, “Implications of the first AMS-02 measurement for dark matter annihilation and decay,” *JCAP* **1311** (2013) 026, [arXiv:1304.1997 \[hep-ph\]](https://arxiv.org/abs/1304.1997).

[9] **DES, Fermi-LAT** Collaboration, A. Albert *et al.*, “Searching for Dark Matter Annihilation in Recently Discovered Milky Way Satellites with Fermi-LAT,” *Astrophys. J.* **834** no. 2, (2017) 110, [arXiv:1611.03184 \[astro-ph.HE\]](https://arxiv.org/abs/1611.03184).

[10] **H.E.S.S.** Collaboration, H. Abdallah *et al.*, “Search for dark matter annihilations towards the inner Galactic halo from 10 years of observations with H.E.S.S.,” *Phys. Rev. Lett.* **117** no. 11, (2016) 111301, [arXiv:1607.08142 \[astro-ph.HE\]](https://arxiv.org/abs/1607.08142).

[11] **Planck** Collaboration, P. A. R. Ade *et al.*, “Planck 2015 results. XIII. Cosmological parameters,” *Astron. Astrophys.* **594** (2016) A13, [arXiv:1502.01589 \[astro-ph.CO\]](https://arxiv.org/abs/1502.01589).

[12] O. Adriani *et al.*, “Measurement of the flux of primary cosmic ray antiprotons with energies of 60-MeV to 350-GeV in the PAMELA experiment,” *JETP Lett.* **96** (2013) 621–627. [Pisma Zh. Eksp. Teor. Fiz. 96, 693 (2012)].

[13] K. Abe *et al.*, “Measurement of the cosmic-ray antiproton spectrum at solar minimum with a long-duration balloon flight over Antarctica,” *Phys. Rev. Lett.* **108** (2012) 051102, [arXiv:1107.6000 \[astro-ph.HE\]](https://arxiv.org/abs/1107.6000).

[14] **AMS** Collaboration, M. Aguilar *et al.*, “Antiproton Flux, Antiproton-to-Proton Flux Ratio, and Properties of Elementary Particle Fluxes in Primary Cosmic Rays Measured with the Alpha Magnetic Spectrometer on the International Space Station,” *Phys. Rev. Lett.* **117** no. 9, (2016) 091103.

[15] G. Giesen, M. Boudaud, Y. Genolini, V. Poulin, M. Cirelli, P. Salati, and P. D. Serpico, “AMS-02 antiprotons, at last! Secondary astrophysical component and immediate implications for Dark Matter,” *JCAP* **1509** no. 09, (2015) 023, [arXiv:1504.04276 \[astro-ph.HE\]](https://arxiv.org/abs/1504.04276).

[16] H.-B. Jin, Y.-L. Wu, and Y.-F. Zhou, “Upper limits on dark matter annihilation cross sections from the first AMS-02 antiproton data,” *Phys. Rev.* **D92** no. 5, (2015) 055027, [arXiv:1504.04604 \[hep-ph\]](https://arxiv.org/abs/1504.04604).

[17] S.-J. Lin, X.-J. Bi, J. Feng, P.-F. Yin, and Z.-H. Yu, “Systematic study on the cosmic ray antiproton flux,” *Phys. Rev.* **D96** no. 12, (2017) 123010, [arXiv:1612.04001 \[astro-ph.HE\]](https://arxiv.org/abs/1612.04001).

[18] A. Reinert and M. W. Winkler, “A Precision Search for WIMPs with Charged Cosmic Rays,” *JCAP* **1801** no. 01, (2018) 055, [arXiv:1712.00002 \[astro-ph.HE\]](https://arxiv.org/abs/1712.00002).

[19] T. Aramaki *et al.*, “Review of the theoretical and experimental status of dark matter identification with cosmic-ray antideuterons,” *Phys. Rept.* **618** (2016) 1–37, [arXiv:1505.07785 \[hep-ph\]](https://arxiv.org/abs/1505.07785).

[20] S. Ting, “The AMS Experiment,” in *AMS Days at La Palma, April 9, Instituto de Astrofísica de Canarias, Spain*. 2018.
<https://http://www.iac.es/congreso/AMSLaPalma2018/>.

[21] S. T. Butler and C. A. Pearson, “Deuterons from High-Energy Proton Bombardment of

Matter,” *Phys. Rev.* **129** (1963) 836–842.

[22] A. Schwarzschild and C. Zupancic, “Production of Tritons, Deuterons, Nucleons, and Mesons by 30-GeV Protons on A-1, Be, and Fe Targets,” *Phys. Rev.* **129** (1963) 854–862.

[23] L. P. Csernai and J. I. Kapusta, “Entropy and Cluster Production in Nuclear Collisions,” *Phys. Rept.* **131** (1986) 223–318.

[24] E. Carlson, A. Coogan, T. Linden, S. Profumo, A. Ibarra, and S. Wild, “Antihelium from Dark Matter,” *Phys. Rev.* **D89** no. 7, (2014) 076005, [arXiv:1401.2461 \[hep-ph\]](https://arxiv.org/abs/1401.2461).

[25] M. Cirelli, N. Fornengo, M. Taoso, and A. Vittino, “Anti-helium from Dark Matter annihilations,” *JHEP* **08** (2014) 009, [arXiv:1401.4017 \[hep-ph\]](https://arxiv.org/abs/1401.4017).

[26] **ALEPH** Collaboration, S. Schael *et al.*, “Deuteron and anti-deuteron production in e+ e- collisions at the Z resonance,” *Phys. Lett.* **B639** (2006) 192–201, [arXiv:hep-ex/0604023 \[hep-ex\]](https://arxiv.org/abs/hep-ex/0604023).

[27] A. Ibarra and S. Wild, “Prospects of antideuteron detection from dark matter annihilations or decays at AMS-02 and GAPS,” *JCAP* **1302** (2013) 021, [arXiv:1209.5539 \[hep-ph\]](https://arxiv.org/abs/1209.5539).

[28] **ALICE** Collaboration, J. Adam *et al.*, “Production of light nuclei and anti-nuclei in pp and Pb-Pb collisions at energies available at the CERN Large Hadron Collider,” *Phys. Rev.* **C93** no. 2, (2016) 024917, [arXiv:1506.08951 \[nucl-ex\]](https://arxiv.org/abs/1506.08951).

[29] **CLEO** Collaboration, D. M. Asner *et al.*, “Anti-deuteron production in Upsilon(nS) decays and the nearby continuum,” *Phys. Rev.* **D75** (2007) 012009, [arXiv:hep-ex/0612019 \[hep-ex\]](https://arxiv.org/abs/hep-ex/0612019).

[30] **BaBar** Collaboration, J. P. Lees *et al.*, “Antideuteron production in $\Upsilon(nS)$ decays and in $e^+e^- \rightarrow q\bar{q}$ at $\sqrt{s} \approx 10.58$ GeV,” *Phys. Rev.* **D89** no. 11, (2014) 111102, [arXiv:1403.4409 \[hep-ex\]](https://arxiv.org/abs/1403.4409).

[31] B. Alper *et al.*, “Large angle production of stable particles heavier than the proton and a search for quarks at the cern intersecting storage rings,” *Phys. Lett.* **46B** (1973) 265–268.

[32] **British-Scandinavian-MIT** Collaboration, S. Henning *et al.*, “Production of Deuterons and anti-Deuterons in Proton Proton Collisions at the CERN ISR,” *Lett. Nuovo Cim.* **21** (1978) 189.

[33] **ALICE** Collaboration, N. Sharma, “Production of nuclei and antinuclei in pp and Pb-Pb collisions with ALICE at the LHC,” *J. Phys.* **G38** (2011) 124189, [arXiv:1109.4836 \[nucl-ex\]](https://arxiv.org/abs/1109.4836).

[34] **ZEUS** Collaboration, S. Chekanov *et al.*, “Measurement of (anti)deuteron and (anti)proton production in DIS at HERA,” *Nucl. Phys.* **B786** (2007) 181–205, [arXiv:0705.3770 \[hep-ex\]](https://arxiv.org/abs/0705.3770).

[35] M.-C. Lemaire, S. Nagamiya, S. Schnetzer, H. Steiner, and I. Tanihata, “Composite particle emission in relativistic heavy ion collisions,” *Physics Letters B* **85** no. 1, (1979) 38 – 42. <http://www.sciencedirect.com/science/article/pii/037026937990772X>.

[36] P. Chardonnet, J. Orloff, and P. Salati, “The Production of antimatter in our galaxy,” *Phys. Lett.* **B409** (1997) 313–320, [arXiv:astro-ph/9705110 \[astro-ph\]](https://arxiv.org/abs/astro-ph/9705110).

[37] **ALICE** Collaboration, S. Acharya *et al.*, “Production of deuterons, tritons, ^3He nuclei and their antinuclei in pp collisions at $\sqrt{s} = 0.9, 2.76$ and 7 TeV,” *Phys. Rev.* **C97** no. 2, (2018) 024615, [arXiv:1709.08522 \[nucl-ex\]](https://arxiv.org/abs/1709.08522).

[38] **STAR** Collaboration, C. Adler *et al.*, “Anti-deuteron and anti-He-3 production in $s(NN)^{**}(1/2) = 130$ -GeV Au+Au collisions,” *Phys. Rev. Lett.* **87** (2001) 262301, [arXiv:nucl-ex/0108022 \[nucl-ex\]](https://arxiv.org/abs/nucl-ex/0108022). [Erratum: Phys. Rev. Lett.87,279902(2001)].

[39] **STAR** Collaboration, H. Agakishiev *et al.*, “Observation of the antimatter helium-4 nucleus,” *Nature* **473** (2011) 353, [arXiv:1103.3312 \[nucl-ex\]](https://arxiv.org/abs/1103.3312). [Erratum: Nature475,412(2011)].

[40] K. Blum, K. C. Y. Ng, R. Sato, and M. Takimoto, “Cosmic rays, antihelium, and an old navy spotlight,” *Phys. Rev. D* **96** no. 10, (2017) 103021, [arXiv:1704.05431 \[astro-ph.HE\]](https://arxiv.org/abs/1704.05431).

[41] T. Sjostrand, S. Mrenna, and P. Z. Skands, “PYTHIA 6.4 Physics and Manual,” *JHEP* **05** (2006) 026, [arXiv:hep-ph/0603175 \[hep-ph\]](https://arxiv.org/abs/hep-ph/0603175).

[42] T. Sjöstrand, S. Ask, J. R. Christiansen, R. Corke, N. Desai, P. Ilten, S. Mrenna, S. Prestel, C. O. Rasmussen, and P. Z. Skands, “An Introduction to PYTHIA 8.2,” *Comput. Phys. Commun.* **191** (2015) 159–177, [arXiv:1410.3012 \[hep-ph\]](https://arxiv.org/abs/1410.3012).

[43] M. Bahr *et al.*, “Herwig++ Physics and Manual,” *Eur. Phys. J.* **C58** (2008) 639–707, [arXiv:0803.0883 \[hep-ph\]](https://arxiv.org/abs/0803.0883).

[44] S. Roesler, R. Engel, and J. Ranft, “The Event generator DPMJET-III at cosmic ray energies,” in *27th International Cosmic Ray Conference (ICRC 2001) Hamburg, Germany, August 7-15, 2001*, pp. 439–442. 2001.
http://www.copernicus.org/icrc/papers/ici6589_p.pdf.

[45] S. Ostapchenko, “QGSJET-II: Towards reliable description of very high energy hadronic interactions,” *Nucl. Phys. Proc. Suppl.* **151** (2006) 143–146, [arXiv:hep-ph/0412332 \[hep-ph\]](https://arxiv.org/abs/hep-ph/0412332).

[46] S. Ostapchenko, “Nonlinear screening effects in high energy hadronic interactions,” *Phys. Rev. D* **74** no. 1, (2006) 014026, [arXiv:hep-ph/0505259 \[hep-ph\]](https://arxiv.org/abs/hep-ph/0505259).

[47] K. Werner, F.-M. Liu, and T. Pierog, “Parton ladder splitting and the rapidity dependence of transverse momentum spectra in deuteron-gold collisions at RHIC,” *Phys. Rev. C* **74** (2006) 044902, [arXiv:hep-ph/0506232 \[hep-ph\]](https://arxiv.org/abs/hep-ph/0506232).

[48] T. Pierog, I. Karpenko, J. M. Katzy, E. Yatsenko, and K. Werner, “EPOS LHC: Test of collective hadronization with data measured at the CERN Large Hadron Collider,” *Phys. Rev. C* **92** no. 3, (2015) 034906, [arXiv:1306.0121 \[hep-ph\]](https://arxiv.org/abs/1306.0121).

[49] S.-J. Lin, X.-J. Bi, and P.-F. Yin, “Expectations of the Cosmic Antideuteron Flux,” [arXiv:1801.00997 \[astro-ph.HE\]](https://arxiv.org/abs/1801.00997).

[50] V. S. Berezinsky, S. V. Bulanov, V. A. Dogiel, and V. S. Ptuskin, *Astrophysics of cosmic rays*. 1990.

[51] A. W. Strong, I. V. Moskalenko, and V. S. Ptuskin, “Cosmic-ray propagation and interactions in the Galaxy,” *Ann. Rev. Nucl. Part. Sci.* **57** (2007) 285–327, [arXiv:astro-ph/0701517 \[astro-ph\]](https://arxiv.org/abs/astro-ph/0701517).

[52] A. W. Strong and I. V. Moskalenko, “Propagation of cosmic-ray nucleons in the galaxy,” *Astrophys. J.* **509** (1998) 212–228, [arXiv:astro-ph/9807150 \[astro-ph\]](https://arxiv.org/abs/astro-ph/9807150).

[53] I. V. Moskalenko, A. W. Strong, J. F. Ormes, and M. S. Potgieter, “Secondary anti-protons and propagation of cosmic rays in the galaxy and heliosphere,” *Astrophys. J.* **565** (2002) 280–296, [arXiv:astro-ph/0106567 \[astro-ph\]](https://arxiv.org/abs/astro-ph/0106567).

[54] A. W. Strong and I. V. Moskalenko, “Models for galactic cosmic ray propagation,” *Adv. Space Res.* **27** (2001) 717–726, [arXiv:astro-ph/0101068 \[astro-ph\]](https://arxiv.org/abs/astro-ph/0101068).

[55] I. V. Moskalenko, A. W. Strong, S. G. Mashnik, and J. F. Ormes, “Challenging cosmic ray propagation with antiprotons. Evidence for a fresh nuclei component?,” *Astrophys. J.* **586** (2003) 1050–1066, [arXiv:astro-ph/0210480 \[astro-ph\]](https://arxiv.org/abs/astro-ph/0210480).

[56] V. S. Ptuskin, I. V. Moskalenko, F. C. Jones, A. W. Strong, and V. N. Zirakashvili, “Dissipation of magnetohydrodynamic waves on energetic particles: impact on interstellar turbulence and cosmic ray transport,” *Astrophys. J.* **642** (2006) 902–916, [arXiv:astro-ph/0510335 \[astro-ph\]](https://arxiv.org/abs/astro-ph/0510335).

[57] M. Korsmeier, F. Donato, and N. Fornengo, “Prospects to verify a possible dark matter hint in cosmic antiprotons with antideuterons and antihelium,” *Phys. Rev.* **D97** no. 10, (2018) 103011, [arXiv:1711.08465 \[astro-ph.HE\]](https://arxiv.org/abs/1711.08465).

[58] L. C. Tan and L. K. Ng, “CALCULATION OF THE EQUILIBRIUM ANTI-PROTON SPECTRUM,” *J. Phys.* **G9** (1983) 227–242.

[59] L. J. Gleeson and W. I. Axford, “Solar Modulation of Galactic Cosmic Rays,” *Astrophys. J.* **154** (1968) 1011.

[60] S. Ting, “Introduction to the AMS Experiment,” in *AMS-02 days at CERN, April 15-17, CERN, Geneva*. 2015. <https://indico.cern.ch/event/381134/timetable/#20150415>.

[61] H.-B. Jin, Y.-L. Wu, and Y.-F. Zhou, “Cosmic ray propagation and dark matter in light of the latest AMS-02 data,” *JCAP* **1509** no. 09, (2015) 049, [arXiv:1410.0171 \[hep-ph\]](https://arxiv.org/abs/1410.0171).

[62] F. Donato, N. Fornengo, D. Maurin, and P. Salati, “Antiprotons in cosmic rays from neutralino annihilation,” *Phys. Rev.* **D69** (2004) 063501, [arXiv:astro-ph/0306207 \[astro-ph\]](https://arxiv.org/abs/astro-ph/0306207).

[63] J. F. Navarro, C. S. Frenk, and S. D. M. White, “A Universal density profile from hierarchical clustering,” *Astrophys. J.* **490** (1997) 493–508, [arXiv:astro-ph/9611107 \[astro-ph\]](https://arxiv.org/abs/astro-ph/9611107).

[64] L. Bergstrom, P. Ullio, and J. H. Buckley, “Observability of gamma-rays from dark matter neutralino annihilations in the Milky Way halo,” *Astropart. Phys.* **9** (1998) 137–162, [arXiv:astro-ph/9712318 \[astro-ph\]](https://arxiv.org/abs/astro-ph/9712318).

[65] B. Moore, S. Ghigna, F. Governato, G. Lake, T. R. Quinn, J. Stadel, and P. Tozzi, “Dark matter substructure within galactic halos,” *Astrophys. J.* **524** (1999) L19–L22, [arXiv:astro-ph/9907411 \[astro-ph\]](https://arxiv.org/abs/astro-ph/9907411).

[66] J. Diemand, B. Moore, and J. Stadel, “Convergence and scatter of cluster density profiles,” *Mon. Not. Roy. Astron. Soc.* **353** (2004) 624, [arXiv:astro-ph/0402267 \[astro-ph\]](https://arxiv.org/abs/astro-ph/0402267).

[67] J. Einasto, “Dark Matter,” in *Astronomy and Astrophysics 2010, [Eds. Oddbjorn Engvold, Rolf Stabell, Bozena Czerny, John Lattanzio], in Encyclopedia of Life Support Systems (EOLSS), Developed under the Auspices of the UNESCO, Eolss Publishers, Oxford ,UK*. 2009. [arXiv:0901.0632 \[astro-ph.CO\]](https://arxiv.org/abs/0901.0632).
<http://inspirehep.net/record/810367/files/arXiv:0901.0632.pdf>.

[68] A. Kounine, “Status of the AMS Experiment,” [arXiv:1009.5349 \[astro-ph.HE\]](https://arxiv.org/abs/1009.5349).

[69] S. Ting, “The First Five Years of the Alpha Magnetic Spectrometer on the International Space Station,” in *CERN Colloquium, December 8, CERN, Zurich*. 2016.

<https://indico.cern.ch/event/592392>.

[70] A. Coogan and S. Profumo, “Origin of the tentative AMS antihelium events,” *Phys. Rev.* **D96** no. 8, (2017) 083020, [arXiv:1705.09664 \[astro-ph.HE\]](https://arxiv.org/abs/1705.09664).